A NUMERICAL AND EXPERIMENTAL STUDY OF THE TRANSMISSION LOSS OF MUFFLERS USED IN RESPIRATORY MEDICAL DEVICES

P. W. Jones and N. J. Kessissoglou

School of Mechanical and Manufacturing Engineering, The University of New South Wales, Sydney NSW 2052, Australia

peter.jones@student.unsw.edu.au, n.kessissoglou@unsw.edu.au

Mufflers are incorporated into continuous positive airway pressure (CPAP) devices to reduce noise in the air paths to and from the flow generating fan. The mufflers are very small, irregularly shaped, and are required to attenuate noise up to 10kHz. It is important that the acoustic performance of these mufflers is reliably predicted and optimised, in order to improve the user experience and maximise compliance with the CPAP therapy. In this study, the acoustic performance of three reactive muffler designs similar to those used in CPAP devices is presented. Transmission loss predictions obtained using analytical and finite element methods are compared with experimental data measured using a test rig based on the two-microphone acoustic pulse method. The analytical methods were found to be unsuitable for predicting the transmission loss of CPAP muffler designs due to the complexity of the muffler geometries. Good agreement between the finite element and experimental results were obtained.

INTRODUCTION AND BACKGROUND

Obstructive sleep apnoea (OSA) is a medical condition whereby the smooth muscles of the upper airway lose sufficient condition during sleep that the airway becomes constricted, resulting in partial or complete obstruction of the airway. OSA can be successfully managed through the application of a positive pressure to the airway during sleep. This elevated airway pressure is produced by a flow generating fan within a continuous positive airway pressure (CPAP) device. Noise from the flow generator is controlled using mufflers situated in the flow path at the fan inlet and the flow generator outlet. The mufflers are very small and are required to attenuate noise up to 10 kHz. Often these mufflers are irregularly shaped and consist of a number of interconnected volumes. They are predominantly reactive, although absorptive materials have been utilised. An assessment of the air path noise characteristics of three ResMed® CPAP device designs has identified that the most significant noise levels are present at frequencies below 4 kHz. This frequency range encompasses the dominant noise sources associated with the rotation of the blower shaft, blade pass frequency and shaft bearing harmonics. With the exception of the narrow peak sound levels associated with these discrete sources, the region of greatest benefit for targeting noise attenuation lies below 1.5 kHz.

The most common type of linear acoustic model used to predict the performance of mufflers applies classical electrical filter theory and is most widely known as the transfer matrix method, although it is also referred to as the two port approach or 4-pole parameter method [1-3]. The acoustic parameters of many of the individual design elements that are frequently used in mufflers have been well characterised [4-6]. Kim and Soedel [7] and Wu *et al*. [8] present a transfer matrix method which rearranges the variables used in the original method such that only the velocity boundary condition is used in the calculation of the matrix parameters. This improved method offers several advantages over the original method when applied with the finite element method to evaluate transmission loss [9]. Other methods include the 3-point method [10] and impedance method (also known as transmission line theory) [11]. Numerical approaches used to predict the performance of mufflers include the finite element method (FEM) [12-14], the boundary element method (BEM) [15, 16], and computational fluid dynamics (CFD) [17]. Barbieri *et al*. [13, 14] implemented the transfer matrix method to predict the acoustic performance of expansion chambers using both the original parameter formulation and the improved method. A comparison of the various numerical methods has been given by Bilawchuk and Fyfe [18].

This study considers the application of the analytical impedance method and transfer matrix method to three reactive muffler designs having dimensions and geometric complexity similar to those found in CPAP devices. These designs correspond to a single expansion chamber design, an integrated multi-chamber design and a multi-chamber design consisting of three interconnected volumes. Acoustic finite element modelling of the designs was conducted by the authors [19] and the results obtained using the ANSYS package are reproduced in this paper. The transmission loss of each of the mufflers was measured using a two-microphone acoustic pulse method which was based on the procedure developed by Seybert and Ross [20]. Experimental results for the three muffler designs are compared with the analytical and computational results.

MUFFLER DESIGNS

The first design shown in Figure 1 consists of a single unbaffled chamber having coaxial inlet and outlet ports. The close proximity between the inlet and outlet ports creates a narrow, short opening between the ports and the muffler chamber. While the level of geometric detail in the design is high, the underlying configuration is that of a Helmholtz resonator. The acoustic characteristics of this design are well known and, as such, it serves as a suitable design for initial comparison between the analytical, computational and

experimental results. The characteristic dimension of the muffler chamber will result in the propagation of some higher order modes within the chamber at frequencies within the desired attenuation range.

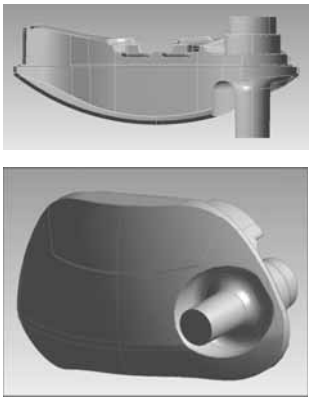

Figure 1: Cross-section and air volume of single chamber design

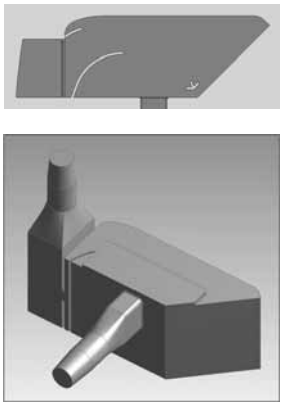

Figure 2: Cross-section and air volume of integrated multi-chamber design

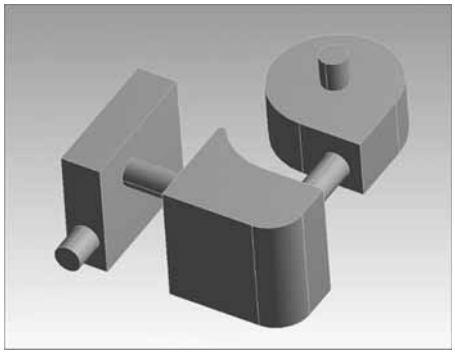

Figure 3: Air volume of three chamber muffler design

The second design shown in Figure 2 consists of two integrated chambers and presents a complex path between the inlet and outlet ports. If air is flowing through the device it would be deflected around a vertical internal baffle before passing through a narrow slot into the final chamber. The third design shown in Figure 3 consists of three interconnected expansion chambers each having orthogonal inlet and outlet ports. The chambers are geometrically simple and contain no internal baffles. A cylindrical pipe of 43mm length and 18mm internal diameter connects each chamber to isolate through-wall noise transmission between adjacent chambers. The dimensions of each muffler design are given in Table 1. The lengths are measured in the direction normal to the chamber inlet and the cross-sectional areas are calculated by dividing the total chamber volume by its length.

Table 1: Dimensions of muffler designs

Design	Chamber 1		Chamber 2		Chamber 3	
	L_1 (mm)	S_1 (mm^2)	L_2 (mm)	S_2 (mm^2)	L_3 (mm)	S_3 (mm^2)
1	35	5,728	-	-	-	-
2	50	6,489	28	2,770	-	-
3	40	5,920	47	7,077	27	7,247

ANALYTICAL APPROACHES

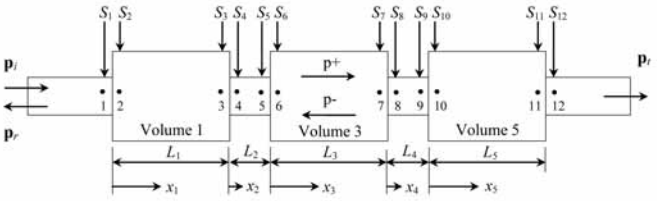

Figure 4: Five volume expansion chamber reactive muffler

Two analytical approaches have been considered: the impedance method and the transfer matrix method. The development of each method is introduced by considering a design comprising three coaxial expansion chambers connected in series by small lengths of pipe, as shown in Figure 4. Unique cross-sectional areas are provided at each point (1 to 12) to allow for the representation of the non-uniform cross-sectional areas that are present in the designs being considered in this study.

Impedance Method

The impedance method is based on the premise that equality of acoustic impedance, Z, is maintained at a change of section. Development of the final equation for transmission loss requires calculating the impedance and pressure at each of the locations 1 to 12 as identified in Figure 4.

Impedance calculations proceed from the outlet (point 12) to the inlet (point 1). The acoustic impedance at point 12 is given by $Z_{12} = z_{12} / S_{12}$, where z_{12} is the specific acoustic impedance and S_{12} is the cross-sectional area of the outlet pipe. By applying an anechoic termination to the outlet duct at point 12, the specific acoustic impedance at that location is equal to the characteristic impedance (ρc), where ρ is the fluid density and c is the speed of sound. Thus the acoustic impedance is given by

$$Z_{12} = \frac{z_{12}}{S_{12}} = \frac{\rho c}{S_{12}} \qquad (1)$$

The acoustic pressures and volume velocities at points 11 and 12 are equal, hence the acoustic impedances at these points are equal. The specific acoustic impedance at point 11 is then given by $z_{11} = Z_{11} S_{11}$ or

$$z_{11} = z_{12} \frac{S_{11}}{S_{12}} \qquad (2)$$

The specific acoustic impedance at point 10 can be found from that at point 11 by considering the impedance formula for undamped plane acoustic waves in a gas column. The complex representation of the actual acoustic pressure is obtained by the superposition of the acoustic pressures associated with the positive and negative travelling one dimensional plane acoustic waves. Thus [2]

$$\mathbf{p}(x,t) = \mathbf{P}_+ e^{j(\omega t - kx)} + \mathbf{P}_- e^{j(\omega t + kx)} \qquad (3)$$

where the amplitude and phase information has been grouped as $\mathbf{P}=Pe^{j\Phi}$. $\mathbf{P}_+$ and $\mathbf{P}_-$ are the complex amplitudes associated with the positive and negative travelling waves, respectively, k is the wave number and ω is the radian frequency. The corresponding particle velocities associated with the positive and negative travelling waves are related to the acoustic pressures by the characteristic impedance. Thus the complex representation of the particle velocity is given by [2]

$$\mathbf{u}(x,t) = \frac{\mathbf{P}_+}{\rho c} e^{j(\omega t - kx)} - \frac{\mathbf{P}_-}{\rho c} e^{j(\omega t + kx)} \quad (4)$$

At $x_5 = L_5$ (corresponding to point 11 in Figure 4), the specific acoustic impedance becomes

$$z_{11} = \frac{\mathbf{p}_{11}}{\mathbf{u}_{11}} = \rho c \left(\frac{\mathbf{P}_+ e^{j(\omega t - kL_5)} + \mathbf{P}_- e^{j(\omega t + kL_5)}}{\mathbf{P}_+ e^{j(\omega t - kL_5)} - \mathbf{P}_- e^{j(\omega t + kL_5)}} \right) \quad (5)$$

which can be rearranged to give

$$\mathbf{P}_- = \mathbf{P}_+ \frac{(1 - \rho c / z_{11})}{(1 + \rho c / z_{11})} e^{-j2kL_5} \quad (6)$$

Similarly, at $x_5 = 0$ (corresponding to point 10 in Figure 4), the specific acoustic impedance can be found as

$$z_{10} = \frac{\mathbf{p}_{10}}{\mathbf{u}_{10}} = \rho c \left(\frac{\mathbf{P}_+ + \mathbf{P}_-}{\mathbf{P}_+ - \mathbf{P}_-} \right) \quad (7)$$

Equations (2), (6) and (7) can be used to show that

$$z_{10} = \rho c \left(\frac{\left(1 + \frac{\rho c S_{12}}{z_{12} S_{11}}\right) e^{jkL_5} + \left(1 - \frac{\rho c S_{12}}{z_{12} S_{11}}\right) e^{-jkL_5}}{\left(1 + \frac{\rho c S_{12}}{z_{12} S_{11}}\right) e^{jkL_5} - \left(1 - \frac{\rho c S_{12}}{z_{12} S_{11}}\right) e^{-jkL_5}} \right) \quad (8)$$

The specific acoustic impedance at point 10 is given by $z_{10} = Z_{10} S_{10}$. The acoustic pressure and volume velocity at points 9 and 10 are equal, hence the acoustic impedances at these points are equal $Z_9 = Z_{10}$. The acoustic impedance at point 9 can then be obtained as

$$Z_9 = \frac{\rho c}{S_{10}} \left(\frac{\left(1 + \frac{\rho c}{Z_{12} S_{11}}\right) e^{jkL_5} + \left(1 - \frac{\rho c}{Z_{12} S_{11}}\right) e^{-jkL_5}}{\left(1 + \frac{\rho c}{Z_{12} S_{11}}\right) e^{jkL_5} - \left(1 - \frac{\rho c}{Z_{12} S_{11}}\right) e^{-jkL_5}} \right) \quad (9)$$

Equation (9) may also be re-stated in non-complex form as

$$Z_9 = \frac{\rho c}{S_{10}} \left(\frac{Z_{12} S_{11} \cos(kL_5) + j\rho c \sin(kL_5)}{\rho c \cos(kL_5) + j Z_{12} S_{11} \sin(kL_5)} \right) \quad (10)$$

The acoustic impedance at points 1 to 8 may be obtained by following the same methodology used in the development of equations (2) to (10), and considering the muffler to comprise five volumes (three expansion chambers plus two interconnecting pipes). The resulting five sets of equations can be combined using the overlap which occurs at the interface between each volume.

Pressure calculations proceed from inlet (point 1) to outlet (point 12). Considering the first volume shown in Figure 4, the pressure and specific acoustic impedance at point 1 are given by

$$\mathbf{P}_1 = \mathbf{P}_i + \mathbf{P}_r \quad , \quad z_1 = \rho c \left(\frac{\mathbf{P}_i + \mathbf{P}_r}{\mathbf{P}_i - \mathbf{P}_r} \right) \quad (11, 12)$$

which can be rearranged to give the acoustic pressure at point 1

$$\mathbf{P}_1 = \frac{2\mathbf{P}_i}{(1 + \rho c / z_1)} \quad (13)$$

Unity pressure amplitude of the incident wave ($\mathbf{P}_i = 1$) has been considered. Equality of the acoustic pressures at points 1 and 2 leads to $\mathbf{P}_2 = \mathbf{P}_1$. At $x_1 = 0$ (corresponding to point 2 in Figure 4), the acoustic pressure given by equation (3) and the specific acoustic impedance can be arranged to give

$$\mathbf{P}_+ = \frac{\mathbf{P}_2 (z_2 + \rho c)}{2 z_2} \quad , \quad \mathbf{P}_- = \frac{\mathbf{P}_2 (z_2 - \rho c)}{2 z_2} \quad (14, 15)$$

The acoustic pressure at point 3 can be obtained from that at point 2 by substituting these relationships into equation (3) defined at point 3 ($x_1 = L_1$).

$$\mathbf{P}_3 = \frac{\mathbf{P}_2}{2} \left((1 + \rho c / z_2) e^{-jkL_1} + (1 - \rho c / z_2) e^{jkL_1} \right) \quad (16)$$

Equality of the acoustic pressures at points 3 and 4 leads to $\mathbf{P}_4 = \mathbf{P}_3$ and, given $z_2 = Z_1 S_2$, the pressure at point 4 can be written in terms of that at point 1 by

$$\mathbf{P}_4 = \frac{\mathbf{P}_1}{2} \left((1 + \rho c / Z_1 S_2) e^{-jkL_1} + (1 - \rho c / Z_1 S_2) e^{jkL_1} \right) \quad (17)$$

Equation (17) may also be re-stated in non-complex form as

$$\mathbf{P}_4 = \frac{\mathbf{P}_1}{Z_1 S_2} (Z_1 S_2 \cos(kL_1) - j\rho c \sin(kL_1)) \quad (18)$$

The acoustic pressure at points 5 to 12 in response to an incident wave of unity pressure amplitude may be obtained by following the same methodology used in the development of equations (16) to (18). As the outlet duct is anechoically terminated, the magnitude of $\mathbf{P}_{12}$ is simply the transmitted pressure, $\mathbf{P}_r$

Transmission loss is calculated using the ratio of the incident acoustic power at the inlet of a system and the transmitted acoustic power at the outlet. The sound power of a travelling harmonic plane acoustic wave is defined as [21]

$$W_{rms} = \int_S \frac{p_{rms}^2}{\rho c} dS \quad (19)$$

p_{rms} is the root mean square pressure and S is the area of the surface through which the sound power is passing. The corresponding form of the transmission loss equation is

$$TL = 10 \log_{10} \left(\frac{W_i}{W_t} \right) \quad (20)$$

W_i and W_t are the incident and transmitted sound power, respectively. For unity pressure amplitude of the incident wave ($\mathbf{P}_i = 1$) the sound transmission loss (TL) for the reactive muffler shown in Figure 4 can now be found from

$$TL = -10 \log_{10} \left(\left| \mathbf{P}_{12}^2 \right| \frac{S_{12}}{S_1} \right) \quad (21)$$

Note that the above derivation accommodates differing cross sectional areas at each of the points 1 to 12. For the simplified case of a single expansion chamber of constant cross section and having inlet and outlet ducts of equal cross section, the above process can be shown to produce a well known form of the transmission loss [20]

$$TL = 10 \log_{10} \left[\cos^2(kL) + \frac{1}{4} \left(\frac{1}{m} + m \right)^2 \sin^2(kL) \right] \quad (22)$$

where m is the expansion ratio (chamber cross section divided by duct cross section).

Transfer Matrix Method

The transfer matrix method (also known as the two port method) uses 2 x 2 matrices to relate two variables at planes on either side of an acoustic component [2]. Matrices for individual components can be readily combined to form a single, overall matrix that describes the behaviour for a multi-component muffler system.

Adopting acoustic pressure (p) and volume velocity (U) as the two state variables, the following general transfer matrix may be written to relate the state variables on either side of an expansion chamber reactive muffler.

$$\begin{bmatrix} p_1 \\ U_1 \end{bmatrix} = \begin{bmatrix} A & B \\ C & D \end{bmatrix} \begin{bmatrix} p_2 \\ U_2 \end{bmatrix} \tag{23}$$

For the case of the simple cylindrical expansion chamber reactive muffler, only the transfer matrices for (i) a uniform tube, (ii) a sudden expansion and (iii) a sudden contraction need to be considered. For a uniform tube, the transfer matrix is given by [2, 4]

$$\begin{bmatrix} A & B \\ C & D \end{bmatrix} = \begin{bmatrix} \cos(kL_c) & j\dfrac{\rho c}{S_c}\sin(kL_c) \\ j\dfrac{S_c}{\rho c}\sin(kL_c) & \cos(kL_c) \end{bmatrix} \tag{24}$$

where L_c is the length of the expansion chamber. When the muffler cross section, S_c, is small compared with the wavelength, and in the absence of air flow, the sudden expansion and contraction at the discontinuities (ends) of the expansion chamber may be represented by simple unit matrices [2]. When this assumption cannot be made, additional elements referred to as "Karal's correction" [5] should be introduced at the discontinuities. The correction matrix is given by

$$\begin{bmatrix} A & B \\ C & D \end{bmatrix} = \begin{bmatrix} 1 & j\omega L_K \\ 0 & 1 \end{bmatrix}, \qquad L_K = \frac{8\rho}{3\pi^2 r_p} H\left(\frac{r_p}{r_c}\right) \tag{25}$$

where L_K is the analogous acoustical inductance, r_p is the radius of the pipe, r_c is the radius of expansion chamber and $H(r_p/r_c)$ is given by Figure 2b in Miwa and Igarashi [5] or may be approximated by

$$H(r_p/r_c) = 0.6857(r_p/r_c)^3 - 0.4312(r_p/r_c)^2 - 1.2501(r_p/r_c) + 1.0006 \tag{26}$$

With reference to the series connected expansion chambers shown in Figure 4, the final transfer matrix, T, can be derived using simple matrix multiplication of the appropriate combination of the above matrices

$$\begin{bmatrix} A_T & B_T \\ C_T & D_T \end{bmatrix} = \begin{bmatrix} 1 & B_{K1,2} \\ 0 & 1 \end{bmatrix} \begin{bmatrix} A_{2,3} & B_{2,3} \\ C_{2,3} & D_{2,3} \end{bmatrix} \begin{bmatrix} 1 & B_{K3,4} \\ 0 & 1 \end{bmatrix} \cdots \begin{bmatrix} A_{10,11} & B_{10,11} \\ C_{10,11} & D_{10,11} \end{bmatrix} \begin{bmatrix} 1 & B_{K11,12} \\ 0 & 1 \end{bmatrix} \tag{27}$$

For the case of a non-reflecting termination of the system, the corresponding form of the transmission loss equation incorporating the transfer matrix constants can be shown to be [2]

$$TL = 20\log_{10}\left[\frac{1}{2}\left(\frac{S_1}{S_{12}}\right)^{1/2}\left(\left|A_T + B_T\left(\frac{S_{12}}{\rho c}\right) + C_T\left(\frac{\rho c}{S_1}\right) + D_T\left(\frac{S_{12}}{S_1}\right)\right|\right)\right] \tag{28}$$

For the simplified case of a single expansion chamber of constant cross section having inlet and outlet ducts of equal cross section and only a very small expansion ratio ($m \sim 1$), the correction matrix given by equation (25) simplifies to become a unit matrix and the above process can be shown to produce the same result as given by equation (22).

As the single chamber design presented in Figure 1 is expected to perform as a Helmholtz resonator rather than a simple expansion chamber, it is appropriate to also consider the transfer matrix for a resonator. Miwa and Igarashi [5] define the transfer matrix parameters for a resonator comprised of a side branch with a closed cavity as:

$$A = D = \cos^2(kL_m) - \sin^2(kL_m) - \frac{\sin(kL_m)\cos(kL_m)}{S_m} R \tag{29}$$

$$\left(B / j\frac{\rho c}{S_m}\right) = 2\sin(kL_m)\cos(kL_m) - \frac{\sin^2(kL_m)}{S_m} R \tag{30}$$

$$\left(C / j\frac{\rho c}{S_m}\right) = 2\sin(kL_m)\cos(kL_m) + \frac{\cos^2(kL_m)}{S_m} R \tag{31}$$

$$R = \frac{S_b \sin(kL_b)\cos(kL_c) + S_c \cos(kL_b)\sin(kL_c)}{\cos(kL_b)\cos(kL_c) - (S_c/S_b)\sin(kL_b)\sin(kL_c)} \tag{32}$$

where L_m is the length of the main pipe extending equally either side of the resonator, S_m is the cross-section of the main pipe, L_b is the length of the side branch (measured from main pipe centreline to start of cavity), S_b is the cross-section of the connecting branch, L_c is the length of the resonator cavity and S_c is the cross-section of the cavity. For the case of a non-reflecting termination of the system, parameters A, B, C and D given by equations (29) to (31) may be substituted into equation (28) to obtain the transmission loss for the resonator.

FINITE ELEMENT APPROACH

Acoustic finite element models of the three muffler designs have been developed using the finite element analysis (FEA) software package ANSYS (Version 11). Transmission loss is calculated by implementing the transfer matrix methodology using ANSYS Parametric Design Language (APDL), a scripting language that may be used to customise the FEA workflow. Kim and Soedel [7] and Wu *et al*. [8] present a method for the calculation of the four pole parameters which presents the general transfer matrix equation in the form

$$\begin{bmatrix} p_1 \\ p_2 \end{bmatrix} = \begin{bmatrix} A^* & B^* \\ C^* & D^* \end{bmatrix} \begin{bmatrix} U_1/S_1 \\ U_2/S_2 \end{bmatrix} \tag{33}$$

S_1, S_2 are the cross-sectional areas of the inlet and outlet pipes, respectively. Utilising this method, the transfer matrix parameters in equation (33) may be calculated by applying the following two load cases

$$\text{Case 1:} \quad A^* = p_1\big|_{u_1=1,\, u_2=0}, \qquad C^* = p_2\big|_{u_1=1,\, u_2=0} \tag{34,35}$$

$$\text{Case 2:} \quad B^* = p_1\big|_{u_1=0,\, u_2=1}, \qquad D^* = p_2\big|_{u_1=0,\, u_2=1} \tag{36,37}$$

where u_1 and u_2 are particle velocities on either side of the acoustic component. It is then possible to calculate the original four pole parameters by combining equations (23) and (33) to give

$$A = \frac{A^*}{C^*} \quad B = \left(B^* - \frac{A^* D^*}{C^*}\right)\left(\frac{1}{S_2}\right) \quad C = \left(\frac{1}{C^*}\right)S_1 \quad D = \left(\frac{-D^*}{C^*}\right)\left(\frac{S_1}{S_2}\right) \tag{38-41}$$

While each load case requires an acoustic particle velocity to be specified, ANSYS does not accept velocity as an applied boundary condition. Instead, the velocity must be converted to a displacement [22] using the relationship $X = -ju / \omega$. The inlet boundary condition can thus be specified with a velocity magnitude equal to unity (u = 1). Acoustic load cases are applied to the finite element model at single frequencies, and analyses are conducted across the frequency range of interest at regular frequency intervals, with the number of computational runs being dictated by the frequency resolution required. The output from the finite element analysis includes the acoustic pressure and particle velocity at each node in the finite element model. The acoustic pressure data from nodes located at the muffler inlet and outlet can be used to calculate the complex transfer matrix parameters using equations (34) to (41). The matrix parameters calculated at each frequency are substituted into equation (28) to obtain the transmission loss spectrum over the desired frequency range.

The finite element model for each muffler design was meshed using tetrahedral FLUID30 elements with mesh controls applied to adequately resolve the fine details and tight radii in the muffler geometries. The resulting mesh size produced 15-25 elements per acoustic wavelength at the upper bound of the frequency range being analysed (limiting case). This is very high compared with a widely accepted minimum acceptable mesh density of 6 elements per wavelength. The fluid (air) was assumed to be non-flowing and inviscid and acoustic damping was not utilised at the fluid-structure interface. That is, the walls were treated as acoustically hard boundaries. The lack of air flow and the absence of both air and structural damping from the models represent a simplification of the actual conditions present in a CPAP device muffler during operation. Further work is being conducted to incorporate damping into the finite element models and to assess the impact of typical CPAP device air flow rates on the acoustic performance of the muffler designs.

EXPERIMENTAL APPROACH

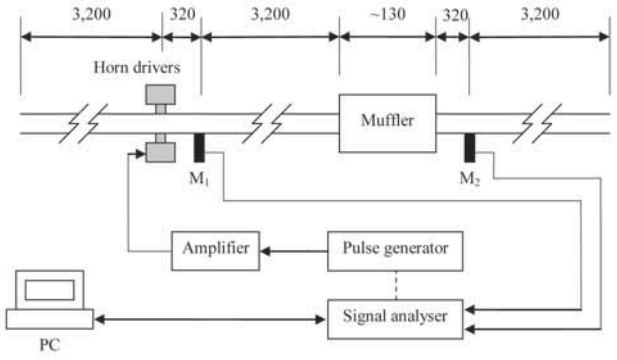

Figure 5: Schematic diagram of the two-microphone acoustic pulse experimental set-up (dimensions are mm)

Experimental data was obtained using a two-microphone technique based on a short duration acoustic pulse [19]. Figure 5 shows a schematic diagram of the experimental set-up used in the current study.

A transient acoustic pulse was generated from the Brüel & Kjær LAN-XI Pulse front end and fed to two TU-650 horn drivers via a PA-25E power amplifier. The pulse propagated down the 18mm diameter PVC conduit where it was measured by the upstream microphone, M_1, before continuing to the muffler inlet. The pressure of the corresponding pulse transmitted from the outlet of the muffler was measured by the downstream microphone, M_2. Utilising long lengths of pipe in the system provided a time separation of approximately 15ms between the arrival of the initial pulse and the arrival of the subsequent reflections of the pulse at the muffler and pipe ends. This time delay was sufficient to facilitate extraction of the time intervals that captured only the initial positive travelling wave from the total time histories recorded by the two microphones. Rectangular windowing with leading and trailing cosine tapers was applied to the time history measured by M_1 and exponential windowing with a leading cosine taper and 5ms decay constant (τ) was applied to the time history measured by M_2. These extracted time histories were captured for 100 individual pulses, Fourier Transformed, and the results averaged in the frequency domain. The transmission loss for the muffler was then obtained using

$$TL = 10\log_{10}\left(\frac{FFT_1}{FFT_2}\right) \tag{42}$$

where FFT_1 and FFT_2 are the Fourier Transforms of the time histories of the incident and transmitted waves, respectively.

RESULTS AND DISCUSSION

Single chamber design

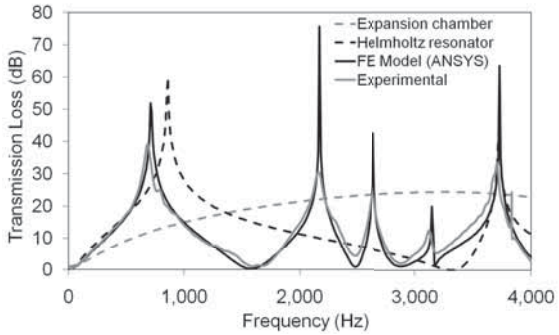

Figure 6: Single chamber muffler comparing analytical (transfer matrix method), FE and experimental results

Figure 6 contains the transmission loss obtained experimentally for the single chamber muffler and the transmission loss predicted by the analytical transfer matrix method (both as an expansion chamber and side branch Helmholtz resonator) and the finite element model. While both analytical models exhibit a poor correlation with the experimental results, the resonator model aligns more closely with the measured results than the expansion chamber model. This is attributed to the close proximity between the coaxial inlet and outlet ports. The FE results show excellent agreement with the experimental results over the frequency range assessed, with the exception that the magnitude at resonant frequencies is over-predicted by the FE model. This is attributed to the FE model assuming an inviscid fluid

and rigid walls. The inclusion of damping in the FE model would result in a reduction in the peaks at the resonances.

Integrated chamber design

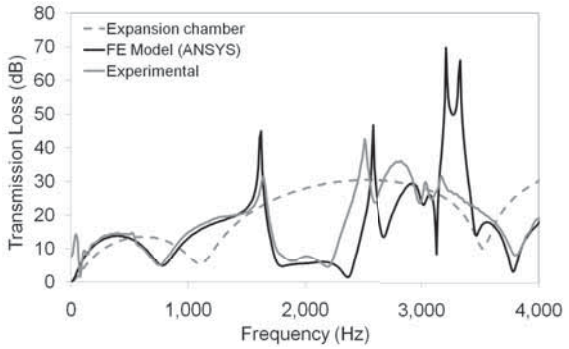

Figure 7: Integrated chamber muffler comparing analytical (transfer matrix method), FE and experimental results

Figure 7 contains the transmission loss obtained experimentally for the integrated chamber muffler and the transmission loss predicted by the analytical transfer matrix method and the finite element model. The analytical approach modelled the muffler chambers as two expansion chambers connected in series. While similarities may be observed, the analytical results show poor agreement with the experimental results. This is attributed to the simplified geometric representation used in the analytical model and the influence of the higher order modes as the frequency increases. The FE results show good agreement up to approximately 3 kHz. The underlying trend followed by both sets of results is similar over the remaining frequency range with the exception of the large double peak predicted by the FE model.

Interconnected chamber design

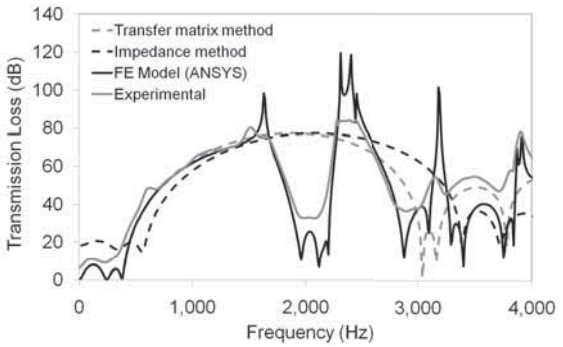

Figure 8: Interconnected chamber muffler comparing analytical (impedance and transfer matrix methods), FE and experimental results

Figure 8 contains the transmission loss obtained experimentally for the interconnected chamber muffler and the transmission loss predicted by the analytical impedance method, the analytical transfer matrix method, and the finite element model. Both analytical methods model the muffler as series-connected expansion chambers. The analytical results show reasonable agreement with the experimental results up to 1.6 kHz, with the transfer matrix method exhibiting closer agreement than the impedance method. Based on a limiting chamber diameter of 95mm, the plane wave cut-on frequency is approximately 2.1 kHz. Application of the analytical approach to this muffler design is complicated by the orthogonal alignment of the inlet and outlet connections on each chamber as the volumes are no longer simply coaxial. While the impedance method provides for differing chamber cross sectional areas at inlet and outlet, both of the analytical methods presented assume one primary path for forward and reverse travelling waves. The FE model results show good agreement with the experimental results for the majority of the frequency range. Departure between the FE results and experimental data at higher frequencies is attributed to assumptions of totally rigid walls and no acoustic damping in the FE model. Altering wall compliance has been shown to significantly affect resonant frequencies in the transmission loss results [23].

During experimental testing, it was noted that pressures in the FFT spectrum for the downstream microphone (M_2) above 500Hz were less than 20 x 10^{-6} Pa, resulting in poor coherence. These observations highlight the importance of producing an acoustic pulse of short duration which still has sufficient energy at high frequencies to provide an acceptable signal-to-noise ratio. A further challenge presented by the two-microphone method is the need to weight the time domain results to capture the initial incident (M_1) and transmitted (M_2) pulses while excluding any subsequent reflections. While use of long lengths of duct goes some way towards providing adequate time spacing, it must be balanced against the higher system losses attributable to the longer ducts. Internal reflection within each of the muffler chambers complicates the separation of the initial transmitted and subsequent reflected pulses due to the length of time decay and lack of clarity in the form of the pressure signal. Care was also required to avoid leakage errors associated with the FFT of the microphone results.

CONCLUSIONS

In this study, the acoustic performance of three reactive muffler designs similar to those used in CPAP devices have been numerically and experimentally compared. Analytical expressions for the transmission loss based on both impedance formulae and the transfer matrix method were developed. Finite element models of the three muffler designs were also generated based on the transfer matrix method. Experimental validation of the computational results was conducted using a test rig based on the two-microphone acoustic pulse method.

At lower frequencies, the analytical results showed reasonable agreement with the finite element and experimental results. However, they departed significantly before reaching the first cut-on frequency, beyond which the plane wave assumption is not valid. The analytical methods are not suitable for CPAP designs due to the complexity of the muffler geometries and the non plane wave behaviour that must be considered when the design incorporates orthogonal inlet and outlet ports.

In general, good agreement between the finite element and experimental results were obtained. The FE models over-predict the transmission loss at resonant frequencies and this is attributed to simplifying assumptions corresponding to the use of inviscid fluid and rigid walls. The experimental results predict that the interconnected chamber design has the most desirable transmission loss characteristics, which is attributed to the combined effect of three discrete chambers, the isolation provided by the interconnecting pipes and a 250% increase in total chamber volume compared to

the single chamber design. The average transmission loss for the integrated chamber design is similar to that of the single chamber design despite a 60% increase in total chamber volume. However, the frequency response is more uniform and the design outperforms the single chamber muffler across much of the frequency range. The proximity between the inlet and outlet ports of the single chamber muffler design results in this design behaving as a Helmholtz resonator, producing narrow transmission loss peaks centred at specific frequencies but having significantly lower performance at other frequencies. Variants of this design may be useful where discrete frequencies are to be targeted but it has limited application over a broad frequency range.

Further refinement of the work covered by this study will include an assessment of the acoustic interaction of adjacent chambers and integration of wall compliance into the FE models. The acoustic performance of the predominantly reactive mufflers used in CPAP devices can be enhanced with the inclusion of dissipative materials. Current work is investigating appropriate experimental techniques for the acoustic characterisation of polyurethane foams with the aim of incorporating significant foam volumes into the muffler FE models.

ACKNOWLEDGMENT

Financial assistance for this work was provided as part of an ARC Linkage Project jointly funded by the Australian Research Council and ResMed.

REFERENCES

[1] Jones, A.D. (1984) "Modelling the exhaust noise radiated from reciprocating internal combustion engines – A literature review", *Noise Control Engineering*, **23**, 12-31.

[2] Munjal, M.L. (1987) *Acoustics of Ducts and Mufflers*, Wiley, New York.

[3] Davies, P.O.A.L. (1988) "Practical flow duct acoustics", *J. Sound and Vibration*, **124**, 91-115.

[4] Igarashi, J. and Toyama, M. (1958) "Fundamentals of Acoustic Silencers: (I) Theory and experiment of acoustic low-pass filters", Report 339, *Aeronautical Research Institute*, University of Tokyo, 223-241.

[5] Miwa, T. and Igarashi, J. (1959) "Fundamentals of Acoustic Silencers: (II) Determination of four terminal constants of acoustical elements", Report 344, *Aeronautical Research Institute*, University of Tokyo, 67-85.

[6] Sullivan, J.W. (1979) "A method for modelling perforated tube muffler components: (I) Theory", *J. Acoust. Soc. America*, **66**, 772-778.

[7] Kim, J. and Soedel, W. (1989) "Analysis of gas pulsations in multiply connected three-dimensional acoustic cavities with special attention to natural mode or wave cancellation effects", *J. Sound and Vibration*, **131**, 103-114.

[8] Wu, T.W., Zhang, P. and Cheng, C.Y.R. (1998) "Boundary element analysis of mufflers with an improved method for deriving the four-pole parameters", *J. Sound and Vibration*, **217**, 767-779.

[9] Barbieri, N., Barbieri, R. and de Lima K.F. (2004) "Errors in transmission loss prediction – the bispectrum and kurtosis approaches", *Mechanical Systems and Signal Processing,* **18**, 223-233.

[10] Wu, T.W. and Wan, G.C. (1996) "Muffler performance studies using direct mixed-body boundary element method and a three-point method for evaluating transmission loss", *J. Vibration and Acoustics*, **118**, 479-484.

[11] Byrne, K.P. (1980) "Calculation of the specific normal impedance of perforated facing-porous backing constructions", *Appl. Acoustics*, **13**, 43-55.

[12] Young C-I.J. and Crocker, M.J. (1975) "Prediction of transmission loss in mufflers by the finite-element method", *J. Acoust. Soc. America*, **57**, 144-148.

[13] Barbieri, R., Barbieri, N. and de Lima K.F. (2004) "Application of the Galerkin-FEM and the improved four-pole parameter method to predict acoustic performance of expansion chambers." *J. Sound and Vibration*, **276**, 1101-1107.

[14] Barbieri, R. and Barbieri, N. (2006) "Finite element acoustic simulation based shape optimization of a muffler", *Appl. Acoustics*, **67**, 346-357.

[15] Cheng, C.Y.R. and Seybert, A.F. (1991) "A multidomain boundary element solution for silencer and muffler performance prediction", *J. Sound and Vibration*, **151**, 119-129.

[16] Selamet, A. and Ji, Z.L. (1999) "Acoustic attenuation performance of circular expansion chambers with extended inlet/outlet", *J. Sound and Vibration*, **223**, 197-212.

[17] Middelberg, J.M, Barber, T.J., Leong, S.S., Byrne, K.P. and Leonardi, E. (2004) "CFD analysis of the acoustic and mean flow performance of simple expansion chamber mufflers", *Proc. ASME Intl. Mechanical Engineering Congress and Exposition*, Anaheim, California.

[18] Bilawchuk, S. and Fyfe, K.R. (2003) "Comparison and implementation of the various numerical methods used for calculating transmission loss in silencer systems", *Appl. Acoustics*, **64**, 903-916.

[19] Jones, P. and Kessissoglou, N. (2009) "An evaluation of current commercial acoustic FEA software for modelling small complex muffler geometries: Prediction vs Experiment", *Proc. ACOUSTICS 2009*, Adelaide.

[20] Seybert, A.F. and Ross, D.F. (1977) "Experimental determination of acoustic properties using a two microphone random-excitation technique", *J. Acoust. Soc. America*, **61**, 1362-1370.

[21] Reynolds, D.R. (1981) *Engineering Principles of Acoustics*, Allyn and Bacon, Massachusetts.

[22] Imaoka, S. (2009) "ANSYS Tips and Tricks: Acoustic Elements and Boundary Conditions", Memo Number *STI:05/01B* [http://ansys.net/?mycat=search&mytype=Tips&mycategory=Sheldon]

[23] Munjal, M.L., Venkatesham, B., Tiwari, M. (2009) "Four-Pole Parameters of a Rectangular Expansion Chamber with Yielding Walls", *Proc. 16th Intl. Congress on Sound and Vibration*, Krakow.